Analysis of a Model for Ship Maneuvering

M. Apri[*]   N. Banagaay[†]   J.B. van den Berg[‡]   R. Brussee[§]
D. Bourne[†]   T. Fatima[†]   F. Irzal[†]   J. Rademacher[¶]
B. Rink[‡]   F. Veerman[‖]   S. Verpoort[**]

Abstract

We analyze numerically and theoretically steady states and bifurcations in a model for ship maneuvering provided by MARIN, and in a simplified model that combines rudder and propeller into an abstract 'thruster'. Steady states in the model correspond to circular motion of the ship and we compute the corresponding radii. We non-dimensionalize the models and thereby remove a number of parameters, so that, due to a scaling symmetry, only the rudder (or thruster) angle remains as a free parameter.

Using 'degree theory', we show that a slight modification of the model possesses at least one steady state for each angle and find certain constraints on the possible steady state configuration. We show that straight motion is unstable for the Hamburg test case and use numerical continuation and bifurcation software to compute a number of curves of states together with their stability, and the corresponding radii of the ship motion. In particular, straight forward motion can be stabilised by increasing the rudder size parameter, and the smallest possible radius is ~ 119 m.

These analyses illustrate methods and tools from dynamical systems theory that can be used to analyse a model without simulation. Compared with simulations, the numerical bifurcation analysis is much less time consuming. We have implemented the model in MATLAB and the bifurcation software AUTO.

1   Introduction

Traditionally, the study of the hydromechanic behaviour of a ship is divided into ship hydrostatics (without motions in calm water), and ship hydrodynamics (with motions in either calm water or in waves or current). The area of ship hydrodynamics can be roughly devided into powering/propulsion and calm water resistance, seakeeping (motions in waves with limited viscous effect) and manoeuvring (motion in calm water).

[*] WUR, Wageningen

[†] TUe, Eindhoven

[‡] VU University Amsterdam

[§] Hogeschool Utrecht

[¶] Centrum voor Wiskunde en Informatica, Amsterdam

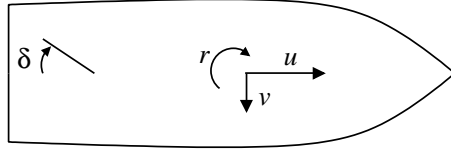[‖] University of Leiden

[**] KU Leuven

Figure 1: Ship-fixed coordinate system with respect to center of mass, and rudder angle notation.

Maneuvring research address the performances of a ship in typical operations such as a zig-zag manoeuvres, turning circles and harbor manoeuvres such as moving sideways or turning on the spot. The actual manoeuvring behaviour of a ship design is investigated in experiments using a scale model. The measured forces and moments are translated into coefficient values for the equations of motion. This allows for numerical simulations which can be used to investigate the manoeuvring behaviour for a variety conditions, such as speed and rudder angle.

In this report we rely on the model provided by MARIN in [7], which we refer to as the 'Rudder model' in the following. It accounts for the forces and moments that act on the center of mass of the ship by water, propeller and rudder. The model uses the reference system of the ship with velocities being surge u, sway v and yaw r. See Figure 1. All forces and moments are given with respect to center of mass, with the longitudinal force denoted by X directed forward according to u, the transverse force Y is directed to starboard according to v, and the rotational force N according to r.

1.1   Equations of motion

Due to the above setup, the framework model reads

$$
\begin{aligned}
(m + m_{uu})\dot{u} &= m\,r\,v + X_H + X_R + X_P \\
(m + m_{vv})\dot{v} + m_{vr}\,\dot{r} &= -m\,r\,u + Y_H + Y_R \\
m_{rv}\,\dot{v} + (I_z + m_{rr})\,\dot{r} &= N_H + N_R,
\end{aligned}
\tag{1}
$$

where all quantities denoted by an m (and I_z) are ship dependent masses and moments of inertia, and the forces and moment X, Y, N have been decomposed into contributions from the hull (H), rudder (R) and propeller (P).

The equations of the force terms for the Rudder model from [7] are given next. These depend on a number of additional ship dependent quantities, such as ρ, L_{pp}, $X'_{u|u|}$, ..., for which we refer to [7]. In terms of u, v, r the forces and moment read

$$X_H = \frac{1}{2}\rho L_{pp}T\left(X'_{u'|u'|}u|u| + X'_{\beta\gamma}L_{pp}v\,r\right) \tag{2}$$

$$Y_H = \frac{1}{2}\rho L_{pp}T\Big(Y'_{\beta}|u|v + Y'_{\gamma}L_{pp}u\,r + Y'_{\beta|\beta|}v|v| + Y'_{\gamma|\gamma|}L_{pp}^2 r|r|$$
$$+ Y'_{\beta|\gamma|}L_{pp}v|r| + Y'_{|\beta|\gamma}L_{pp}|v|r + Y'_{ab}\,|u^{ay}v^{by}|\,\mathrm{sign}(v)V^{-ay-by+2}\Big) \tag{3}$$

$$N_H = \frac{1}{2}\rho L_{pp}^2 T\Big(N'_{\beta}u\,v + N'_{\gamma}L_{pp}r|u| + N'_{u'\gamma c}L_{pp}^{c_n}|u\,r^{c_n}|V^{-c_n+1}\mathrm{sign}\,r$$
$$+ N'_{\gamma|\gamma|}r|r|L_{pp}^2 + N'_{\beta|\beta|}v|v| + N'_{\beta\beta\gamma}r\,v^2 L_{pp}V^{-1}$$
$$+ N'_{\beta\gamma\gamma}v\,r^2 L_{pp}^2 V^{-1}\mathrm{sign}\,u + N'_{ab}|u^{a_n}v^{b_n}|V^{-a_n-b_n+2}\mathrm{sign}\,(u\,v)\Big) \tag{4}$$

$$X_P = (1-t)T_p(u),\; T_p(u) = \sum_{i=0}^{5}K_{T_i}\left(\frac{u(1-w)}{nD_p}\right)^i\rho n^2 D_p^4. \tag{5}$$

$$X_R = -\frac{1}{2}\rho V_{rr}^{-1}A_R C_L\Big(\frac{C_L u_r}{\pi\Lambda}(u_r\sin\delta - v_r\cos\delta)^2 \tag{6}$$
$$+ v_r(u_r\sin\delta - v_r\cos\delta)(u_r\cos\delta + v_r\sin\delta)\Big)$$

$$Y_R = \frac{1}{2}(1+a_H)\rho V_{rr}^{-1}A_R C_L\Big(u_r(u_r\sin\delta - v_r\cos\delta)(u_r\cos\delta + v_r\sin\delta) \tag{7}$$
$$- \frac{C_L v_r}{\pi\Lambda}(u_r\sin\delta - v_r\cos\delta)^2\Big)$$

$$N_R = Y_R\,x_r - X_R\,y_r \tag{8}$$

where

$$V_{rr} = \sqrt{u_r^2 + v_r^2}$$
$$u_r = u_p + C_{rue}\left(\sqrt{u_p^2 + \frac{8T_p(u)}{\rho\pi D_p^2}} - u_p\right)$$
$$v_r = C_{db}\,v + C_{dr}\,x_r\,r$$
$$u_p = (1-w)u$$

Strictly speaking, the rudder forces are given for the case of forward speed with positive thrust. For other courses these need to be modified.

Note that while u, v are velocities with dimension m/s, the third component r is an angular velocity with dimension $1/s$. The first two force equations $(1)_1$ and $(1)_2$ are therefore nondimensionalised by the factor $\frac{1}{2}\rho V^2 L_{pp}T$ with $[\rho] = $ kg/m³, $[V] = $ m/s, $[L_{pp}] = [T] = $ m. The moment equation $(1)_3$ is therefore nondimensionalised by the factor $\frac{1}{2}\rho V^2 L_{pp}^2 T$, since $[N_i] = $ N·m. This yields a system of non-dimensional quantities of the form

$$\mathbf{M}\dot{\mathbf{w}} = \mathbf{f}(\mathbf{w}). \tag{9}$$

Remark. *For the analysis of the equations of motion it is important to note that the model becomes invalid near $u = 0$. Indeed, the hull moment N_H is discontinuous due*

to the term

$$L_{pp}^2 N'_{\beta\gamma\gamma}\text{sign}(u)vR^2/V, \tag{10}$$

which is inconvenient for the analysis, and partly for the numerics as it causes degeneracies.

Moreover, according the model given in [7], the form of the rudder forces actually changes for backward motion. Hence, solutions to the model used in this report with negative or vanishing u are not necessarily meaningful for the practical application. However, we mostly ignore this aspect as we strive for a theoretical analysis and the demonstration of our methods in this report.

1.1.1   Thruster model

Due to the complexity of the full 'Rudder model' and in order to isolate the influence of the hull forces, we introduce a simplified "Thruster model," where the propeller and rudder forces are combined into an effective force acting on the hull that may be interpreted as a thruster.

Thus we replace $X'_P + X'_R$ and Y'_R, N'_R by abstract forces X'_T, Y'_T, N'_T, respectively, where

$$
\begin{aligned}
X'_T &= \tau\cos\alpha \\
Y'_T &= \tau\sin\alpha \\
N'_T &= x'_r\tau\sin\alpha,
\end{aligned}
$$

which means there is force of amplitude τ acting at angle α on the hull. The (non-dimensionalized) equations of motion read

$$
\begin{aligned}
(m' + m'_{uu})\dot{u} &= m'Rv + X'_H + \tau\cos(\alpha) \\
(m' + m'_{vv})\dot{v} + m'_{vr}\dot{R} &= -m'Ru + Y'_H + \tau\sin(\alpha) \\
m'_{rv}\dot{v} + (I'_z + m'_{rr})\dot{R} &= N'_H + x'_r\tau\sin(\alpha).
\end{aligned}
\tag{11}
$$

where $R = L_{pp}r$. A notable difference to the full Rudder model is that here the propeller acts in a direction given by α, while the propeller in the Rudder model always pushes at angle zero. Moreover, the Rudder model does not distinguish rudder angles that differ by $180°$; the forces are the same, whether rudder points towards the stern or the aft. This is not so in the Thruster model, and indeed the results are quite different for angles around $180°$.

2   Theoretical analysis

2.1   Interpretation of equations and steady states

Written compactly, the model equations are of the form

$$\mathbf{M}\dot{\mathbf{w}} = \mathbf{f}(\mathbf{w}), \tag{12}$$

which is a so-called algebro-differential equation as the left hand side is multiplied by a matrix. We will assume that, as in the Hamburg test case, the mass matrix is invertible so that we can rewrite (12) as the ordinary differential equation system

$$\dot{\mathbf{w}} = \mathbf{M}^{-1}\mathbf{f}(\mathbf{w}). \tag{13}$$

(If the mass matrix is not invertible the analysis become much more subtle.)

Steady states (also referred to as *equilibria*) of the differential equations are such that the time derivatives vanishing, that is, equilibria solve the non-linear algebraic equation

$$0 = \mathbf{f}(\mathbf{w}). \tag{14}$$

The set of solutions to this equation can be rather complicated and cannot easily be determined. Indeed, much of this report is dedicated to the existence and structure of solutions to (14).

A special steady state solution can, however, be found immediately: Since the equations model ship motion, for a straight rudder $\delta = 0$ or ($\alpha = 0$ for the Thruster model), there is a steady state where sway and yaw are zero ($r = v = 0$) –yielding straigh motion– and the surge is adjusted according to propeller or thruster settings. See Section 2.2.2 for details on this course for the Thruster model.

The question arises what the course of the ship is at other steady states. This requires to change from the ship reference system to a reference system (x, y) of a standing observer. It turns out that, for a ship in a steady state (14), the observer can always be placed so that a ship that moves in a circle around the observer. To see this intuitively, note that the sum of the constant surge and sway generates drift in a fixed direction. The yaw generates a superimposed rotation so that the overall motion is a pure rotation.

Mathematically, it is convenient to use complex numbers and write $w = u + iv$ for the drift term and $z = x + iy$ for the observer coordinates. Let ϕ denote the orientation angle of the ship. Then

$$\dot{z} = w e^{i\phi} \tag{15}$$

$$\dot{\phi} = \omega := r + \arg(w), \tag{16}$$

and so $\phi = \omega t + \phi(0)$, which gives

$$z = z(0) + \left(\frac{w e^{i\phi(0)}}{i\omega} \right) e^{i\omega t}, \tag{17}$$

which is circular motion with radius $|w|/\omega$ and angular velocity ω.

Having found a steady state, the question is whether the ship can by itself follow this course, that is, whether perturbations from the steady state decay or at least do not grow. This is referred to as *stability* of the steady state. For ordinary differential equations stability of equilibria is essentially determined by the eigenvalues of the linearization of the right hand side evaluated in the steady state. In (13) this linearisation is the Jacobian matrix $\mathbf{M}^{-1} Df$. It is well known in nonlinear dynamical systems theory that:

- If the real parts of all eigenvalues are negative, then the equilibrium is stable: all small perturbations decay exponentially in time (with rate given by the largest of the negative real parts).

- If one of the eigenvalues has positive real part, then the steady state is unstable in the sense that all generic perturbations will drive the solution away from the equilibrium.

- The marginal case when all real parts are non-positive with one or more on the imaginary axis typically gives rise to a bifurcation. Roughly speaking bifurcation means that the set of bounded solutions changes qualitatively.

Rudder model.   Before focussing on the simpler Thruster model, we remark that, for small propeller and rudder forces, the results on existence and stability of straight motion from the Thruster model carry over to the Rudder model. For instance, if the rudder area and propeller are small compared with $L_{pp}T$, then the hull forces dominate. For instance, in the numerical analysis of the Rudder model we find that straight motion is unstable, which we can show by pencil and paper for the Thruster model.

We briefly consider the 'turn on the spot' maneuver, which means $u = v = 0$, $R \neq 0$. As we will see in the next section, this maneuver is typically impossible in equilibrium for the Thruster model. Here we show that the same holds for the Rudder model with rudder at the symmetry axis of the hull, that is, $y_r' = 0$.

For $u = v = 0$, the first equation, (1) implies that $X_P' + X_R' = 0$. The second and third equation imply $0 = Y_R' + Y_{\gamma|\gamma|}' R|R|$, $0 = N_R' + N_{\gamma|\gamma|}' R|R|$. The symmetric rudder location $y_r' = 0$ implies $N_R' = Y_R' x_r'$ and we infer

$$Y_R'(Y_{\gamma|\gamma|}' x_r' - N_{\gamma|\gamma|}') = 0.$$

Now, $Y_R' = 0$ implies $R = 0$, which corresponds to a static equilibrium. On the other hand, $Y_{\gamma|\gamma|}' x_r' \neq N_{\gamma|\gamma|}'$ for typical values of these ship dependent constants, which means that this maneuver is typically impossible in equilibrium.

2.2   Thruster model

In this section we analyze some aspects of the Thruster model. On the one hand we discuss stability and bifurcation of the simple straight forward motion, show non-existence of 'turn on the spot', and in particular discuss an abstract way to obtain insight into existence of equilibria. Due to the abstract nature of the model, we are not concerned with units and comparison with realistic values for the solutions we find.

We start out with noting symmetries of the Thruster model equations. The (u, r, v)-dependent terms on the right hand side are all homogeneous of degree 2 in the sense that rescaling $(u, R, v) \rightarrow \lambda(u, R, v)$ with $\lambda \geq 0$ yields the same terms multiplied by λ^2. This means that for $\lambda = \sqrt{\tau}$, a time rescaling removes the parameter τ from the problem – except when it is zero, which we exclude in the following.

In addition to this scaling symmetry, the equations possess the symmetry

$$(\alpha, u, v, r) \rightarrow (-\alpha, u, -v, -r), \tag{18}$$

which means that any equilibrium has a symmetric partner for opposite thruster angle and is a result of the effective reflection symmetry of hull and thruster.

2.2.1   Non-existence of "turn on the spot"

In this section we show that as in the Rudder model, equilibria with $u = v = 0$ and $R \neq 0$ typically do not exist. Again we set $\dot{u} = \dot{v} = \dot{R} = 0$ in (11) to identify equilibria.

Substituting $u = v = 0$ into the first equation of (11) gives $0 = \tau \cos(\alpha)$, which implies either $\tau = 0$ (which is uninteresting) or $\alpha = (2k + 1)\pi/2$ for some integer k (which means a $\pm 90°$ rudder angle).

Substituting $u = v = 0$ in the second and third equation implies

$$0 = Y'_{\gamma|\gamma|} R|R| + \tau \sin(\alpha)$$
$$0 = N'_{\gamma|\gamma|} R|R| + x'_r \tau \sin(\alpha).$$

The case $\tau = 0$ immediately implies $R = 0$, and for the case $\alpha = (2k + 1)\pi/2$, we have $R|R| = -\tau \sin(\alpha)/Y'_{\gamma|\gamma|}$, which yields the condition

$$N'_{\gamma|\gamma|}/Y'_{\gamma|\gamma|} = x'_r,$$

which already appeared in the Rudder model. For generic values of the ship constants this is not true. Theoretically, one may view x'_r as an independent parameter so that the above constraint shows where to put the rudder in order to have a ship that is able to perform pure rotational motion in equilibrium for fully sideways thruster.

2.2.2   Stability of straight motion

Straight motion in equilibrium is a solution to (11) with vanishing left hand side and $v = r = 0$. Equations $(11)_{2,3}$ imply $\alpha = 0$ and from $(11)_1$ it follows that $u = u(\tau)$ is the unique solution to

$$X'_{u'|u'|} u|u| + \tau = 0.$$

Hence, for $X'_{u'|u'|} \neq 0$, $u = 0$ if and only if $\tau = 0$, which we do not consider here. In particular,

$$\mathrm{sign}(u) = -\mathrm{sign}(\tau X'_{u'|u'|}), \quad |u| = \sqrt{|\tau/X'_{u'|u'|}|}.$$

The linearisation in $r = v = 0$ of the right hand side of (11) reads

$$\begin{pmatrix} \partial_u X'_H & 0 & 0 \\ 0 & \partial_v Y'_H & \partial_r Y'_H \\ 0 & \partial_v N'_H & \partial_r N'_H \end{pmatrix} = \begin{pmatrix} 2X'_{u'|u'|}|u| & 0 & 0 \\ 0 & Y'_\beta|u| & (Y'_\gamma - m')u \\ 0 & N'_\beta u & N'_\gamma|u| \end{pmatrix}$$

where partial derivatives are evaluated at $r = v = 0$.

In order to derive stability properties this must be multiplied by the inverse of the mass matrix on the left hand side of (11) given by

$$\begin{pmatrix} m' + m'_{uu} & 0 & 0 \\ 0 & m' + m'_{vv} & m'_{vr} \\ 0 & m'_{rv} & I'_z + m'_{rr} \end{pmatrix}^{-1} =$$

$$D^{-1} \begin{pmatrix} D(m' + m'_{uu})^{-1} & 0 & 0 \\ 0 & I'_z + m'_{rr} & -m'_{rv} \\ 0 & -m'_{vr} & m' + m'_{vv} \end{pmatrix}.$$

Here $D = (m' + m'_{vv})(I'_z + m'_{rr}) - m'_{rv}m'_{vr}$ is the determinant of the lower right 2-by-2 submatrix of the mass matrix for (r, v). For the Hamburg test case, $D = 0.06$. In that case also $X'_{u'|u'|} < 0$, which is natural as it means that the acceleration in the hull direction will adjust to the force balance given by the thrust that acts in that direction; at least on the linear level.

Therefore, stability is determined by the (r, v)-submatrix, which measures the effects of perturbations in the v- and r-directions. The matrix reads

$$S := \begin{pmatrix} I'_z + m'_{rr} & -m'_{rv} \\ -m'_{vr} & m' + m'_{vv} \end{pmatrix} \begin{pmatrix} Y'_\beta|u| & (Y'_\gamma - m')u \\ N'_\beta u & N'_\gamma|u| \end{pmatrix} =$$
$$\begin{pmatrix} (I'_z + m'_{rr})Y'_\beta|u| - m'_{rv}N'_\beta u & (I'_z + m'_{rr})(Y'_\gamma u - m') - m'_{rv}N'_\gamma|u| \\ -m'_{vr}Y'_\beta|u| + (m' + m'_{vv})N'_\beta u & -m'_{vr}(Y'_\gamma - m')u + (m' + m'_{vv})N'_\gamma|u| \end{pmatrix}.$$

Trace and determinant are

$$\text{tr}(S) = ((I'_z + m'_{rr})Y'_\beta + (m' + m'_{vv})N'_\gamma)|u| - (m'_{rv}N'_\beta + m'_{vr}(Y'_\gamma - m'))u$$
$$\det(S) = D(Y'_\beta N'_\gamma - N'_\beta(Y'_\gamma - m'))u^2.$$

The masses are always positive. For the Hamburg test case these and the hydrodynamic hull constants are

$$m' = 0.2328, m'_{vv} = 0.2286, m'_{rv} = m'_{vr} = 0.0074, I'_z + m'_{rr} = 0.0284,$$
$$Y'_\beta = -0.1735, Y'_\gamma = 0.0338, N'_\beta = -0.1442, N'_\gamma = -0.0267.$$

In particular, (keeping four digits)

$$\text{tr}(S) = (-\text{sign}(u)0.0174 + 0.0025)u < 0,$$
$$\det(S) = 0.0601(-0.0240)u^2 = -0.0014u^2 < 0.$$

Since the determinant (product of eigenvalues) is negative, eigenvalues are real with opposite signs. The negative trace means that the positive eigenvalue is smaller than the negative in absolute values. In this case eigenvalues are (to three digits) -0.027 and 0.012.

In particular, the positive eigenvalue means that equilibrium straight motion for the Hamburg test case is *unstable*, which makes sense for a hull to aid manoeuvering. The eigenvector associated to the unstable eigenvalue 0.012 is $(0.331, -0.94)$, which means that the main effect of the instability is a rotation in negative r direction; the smaller effect is a sideways shift in positive v-direction.

2.2.3 Theoretical stability change

At least from a theoretical viewpoint, it is instructive to study which of the ship parameters can change stability of straight motion. It turns out that one way is by varying m' only, keeping other values the same. In practice this may be impossible as other ship constants may change when m' changes. Nevertheless, this sheds light on the possible bifurcation structures.

Trace and determinant in that case read

$$\text{tr}(S) = (-\text{sign}(u)(0.0111 + 0.0267m') + 0.0008 + 0.0074m')u < 0,$$
$$\det(S) = (0.00003 + 0.0017m' - 0.0350(m')^2)u^2.$$

Since the trace remains always negative, a stability change must occur at vanishing determinant. Recall that positive determinant for negative trace means both eigenvalues are negative (or have negative real part) and therefore imply stability of the equilibrium straight motion.

Since the determinant is quadratic in m' and positive at $m' = 0$, it is positive only in an interval including $m' = 0$, and negative for all other values of m'. The Hamburg test case has negative determinant and therefore m' must be decreased to generate a stable equilibrium straight motion. This may be counter-intuitive as this suggest decreasing hulls weight generates stability. However, in practice it may be impossible to change m' alone as modification of the design likely effect other parameters as well.

In nonlinear systems such as (11), a stability change by a real eigenvalue implies bifurcation of other equilibrium solutions as discussed in the next section.

2.3 Stability analysis of the simple thruster model

The equation of motion are

$$(m + m_{uu})u' = mrv + X_G$$
$$(m + m_{vv})v' + m_{vr}r' = -mru + Y_G$$
$$m_{rv}v' + (I_z + m_{rr})r' = N_G,$$

where $m_{vr} = m_{rv}$. Here $(X_G, Y_G, N_G) = (X_H + X_T, Y_H + Y_T, N_H + N_T)$ are composed of the hull forces/moments and thruster forces/moments. The former are given, in slightly simplified form, by

$$X_H = X_{uu}u|u| + X_{\beta\gamma}vr$$
$$Y_H = Y_\beta|u|v + Y_\gamma ur + Y_{\beta\beta}v|v| + Y_{\gamma\gamma}r|r| + Y_{\beta\gamma}v|r| + Y_{\gamma\beta}|v|r$$
$$N_H = N_\beta uv + N_\gamma r|u| + N_{\gamma\gamma}r|r| + N_{\beta\beta}v|v|.$$

In our simple thruster model we have

$$X_T = \tau \cos \alpha$$
$$Y_T = \tau \sin \alpha$$
$$N_T = \tau x_\tau \sin \alpha,$$

where x_τ is the position of the thruster (relative to the center of mass), τ is the magnitude of the trust force, and α its angle.

For $\alpha = 0$ we linearize around the straight motion $(u, v, r) = (u_0, 0, 0)$, with $u_0 = \sqrt{-\tau/X_{uu}}$, where $X_{uu} < 0$. The linearized equations are

$$
\begin{bmatrix}
m + m_{uu} & 0 & 0 \\
0 & m + m_{vv} & m_{vr} \\
0 & m_{rv} & I_{zz} + m_{rr}
\end{bmatrix}
\begin{bmatrix}
u' \\
v' \\
r'
\end{bmatrix} =
$$
$$
\begin{bmatrix}
2X_{uu}u_0 & 0 & 0 \\
0 & Y_\beta u_0 & (-m + Y_\gamma)u_0 \\
0 & N_\beta u_0 & N_\gamma u_0
\end{bmatrix}
\begin{bmatrix}
u \\
v \\
r
\end{bmatrix}.
$$

Clearly, the stability of $(u_0, 0, 0)$ depends on the matrix

$$\left[\begin{array}{cc} Y_\beta & (-m + Y_\gamma) \\ N_\beta & N_\gamma \end{array} \right]. \tag{19}$$

Typical (suitably nondimensionalized) values for the parameters are

$$Y_\beta = -0.2, \quad Y_\gamma = 0.03, \quad N_\beta = -0.1, \quad N_\gamma = -0.03, \quad m = 0.2,$$

for which the determinant and trace of (19) are negative: this means that this 2×2 submatrix has one positive and one negative eigenvalue. Thus, the solution $(u, v, r) = (u_0, 0, 0)$ is unstable. For smaller values of m the determinant becomes positive, while the trace remains negative. Hence, the point $(u_0, 0, 0)$ can become stable if one changes parameters.

We remark that the ship's left-right symmetry implies that its equations of motion are symmetric under the map $S : (u, v, r) \mapsto (u, -v, -r)$, see (18).

The generic scenario in which a stationary point of a smooth vector field with the above symmetry loses stability is the pitchfork bifurcation. Because the equations of motion of the ship are not smooth - due to the dissipative terms of the form $u|u|$ and so on - a model for the bifurcation in question is described by the local normal form

$$\frac{dx}{dt} = f_\pm(x, \lambda), \text{ with } f_\pm : \mathbb{R} \times \mathbb{R} \to \mathbb{R} \text{ defined by } f_\pm(x, \lambda) := x(\lambda \pm |x|).$$

Note that the symmetry of this differential equation is reflected by $f_\pm(-x, \lambda) = -f_\pm(x, \lambda)$.

It is clear that $x = 0$ is an equilibrium point for $f_\pm$ for all values of the parameter λ. The linearized differential equation $\frac{dx}{dt} = \lambda x$ shows that this point is stable for $\lambda < 0$ and unstable for $\lambda > 0$. Moreover, on one side of the bifurcation point $\lambda = 0$, two extra stationary solutions exist, given by $x = \pm \lambda$. These branches emerge from the point $(x, \lambda) = (0, 0)$. For f_- they exist for $\lambda > 0$, which is why f_- is called a "supercritical pitchfork". These additional equilibria are stable. f_+ is called a subcritical pitchfork, because the extra solutions exist for $\lambda < 0$. They are unstable. Figure 2 is the bifurcation diagram for f_-, that summarizes this information. Figure 2 should be compared with numerical results that were obtained for the thruster model. It shows a nearly exact match with the theory.

For completeness, we have also indicated the local degree of the solutions. Note that the total degree is always equal to -1. The concept of degree will be explained in the next section. It will also be explained in the next section that an unstable straight motion can never exist alone. This provides a topological explanation of why in the above non-smooth pitchfork bifurcation, two stable solutions are born.

2.4 Degree theory: Existence of Equilibria

The ship models we have considered sofar can be written in the following general form

$$M\dot{\vec{v}} = F(\vec{v}, \alpha) = F^\perp(\vec{v}) + F_D(\vec{v}, \alpha) + F_T(\vec{v}, \alpha),$$

where $\vec{v} = (u, v, Lr)$, M is an invertible symmetric matrix with the dimension of mass, $F^\perp(\vec{v}) = (mrv, -mru, 0)$ is the Coriolis force coming from the choice of
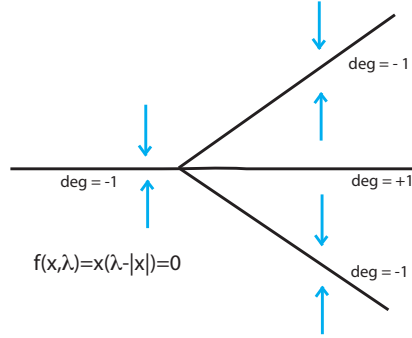
Figure 2: Bifurcation diagram of $\frac{dx}{dt} = f_-(x, \lambda) = x(\lambda - |x|)$.

rotating coordinates, F_D is a dissipative force from friction and viscosity, and F_T is a thrusting force. We have a certain freedom in the way we split up a force in a F_D and F_T part. In particular, for the rudder model there is a term $F_D(\vec{v}, \delta)$ and a thruster force $F_T(u)$ which is a bounded function of u, whereas in the steerable thruster model there is the assumption that $F_D = F_D(\vec{v})$ depends only on the velocity and $F_T = F_T(\alpha)$ is a constant that only depends on a steering angle. All forces implicitly depend on design parameters. We sometimes suppress the steering angle α, as for our purposes it can be considered a fixed parameter just like the design parameters.

There is a fundamental physical reason for splitting up the forces. We make assumption that for very large velocities the dissipative force will give a kinetic energy loss that dominates the thrust force. Of course in this statement the precise meaning of very large may depend on parameters like the power generated by the engines. Thus, this assumption is very mild. Since the mass matrix is symmetric, the change in kinetic energy per second can be computed as

$$
\begin{aligned}
\frac{d}{dt} E_{kin} &= \frac{1}{2} \frac{d}{dt} \vec{v} \cdot M \vec{v} \\
&= \frac{1}{2} (\dot{\vec{v}} \cdot M \vec{v} + \vec{v} \cdot M \dot{\vec{v}}) \\
&= \vec{v} \cdot M \dot{\vec{v}} \\
&= \vec{v} \cdot (F_D + F_T),
\end{aligned}
$$

where in the last line we used that the Coriolis force is orthogonal to the velocity vector $\vec{v}$.

A precise formulation of the assumption we make is the following. For $V_0 > 0$ let

$$
S^2(V_0) = \{\vec{v} \in \mathbb{R}^3 \mid \|\vec{v}\| = V_0\}
$$

be the 2-sphere with radius V_0. It bounds the 3-ball $B^3(V_0) = \{\vec{v} \in \mathbb{R}^3 \mid \|\vec{v}\| \le V_0\}$. Here it is easiest to think of the normal round sphere but if we wish, we can choose the norm $\|\cdot\|$ to define the sphere $S^2(V_0)$ at our convenience e.g. we could define $\|\vec{v}\| = \max(|u|, 12.34|v|, 5.678|Lr|)$ if the region of interest is defined by different upper bounds for forward, transverse and yaw velocities.

Assumption 2.1. *If V_0 is sufficiently large then for all velocities $\vec{v} \in S^2(V_0)$ the kinetic energy decreases i.e.*

$$\vec{v} \cdot F = \vec{v} \cdot (F_D + F_T)(\vec{v}) < 0$$

We should explain what sufficiently large means. The condition is physically very natural, if not inevitable. For the model, however, it suffices that the assumption is true for V_0 somewhat larger than the velocities of a ship at maximum thrust. We really only assume that the model is physically acceptable for high, but not for insanely high velocity ranges. For example, if the model contains small high order polynomial corrections that, when blindly extrapolated to absurdly high velocities, become leading order and ruin the assumption, that does not matter. In fact, it is best to assume it is only defined for $\|\vec{v}\| \leq V_0$. Mathematically the point is that on the boundary of the velocity range of interest the force field is pointing inwards. We also assume that it is topologically a three-dimensional ball bounded by a 2-sphere, but that could be relaxed.

2.4.1   Existence result

The *flow* $\Phi_F^t(\vec{v})$ of the vector field $F(\vec{v})$ is the solution of the equation $\dot{w} = F(w)/1kg$ with boundary condition $w_0 = \vec{v}$. If the vector field is continuous its flow is also continuous for short times. The fixed points of the flow for $t > 0$ are exactly the zeros of F i.e. the equilibria. Now a reformulation of assumption 2.1 is that F is inward pointing on the sphere $S^2(V_0)$. It follows that the flow Φ_F^t can never leave the ball $B^3(V_0)$ and maps the ball to itself, i.e. for fixed t the flow can be restricted to a continuous map

$$\Phi_F^t : B^3(V_0) \to B^3(V_0).$$

By the Brouwer fixed point theorem, a continuous map from the ball to itself always has a fixed point. Therefore, an equilibrium always exists.

2.4.2   There are -1 Equilibria

The Brouwer fixed point theorem is one of the first and best known examples of the use of algebraic topology in analysis. Using a tiny bit of algebraic topology directly we can make a much more precise quantitative statement about the number of equilibria *counted with multiplicity*. In particular we will be able to state what we mean by multiplicity and it turns out that negative multiplicities have to be allowed.

The counting of equilibria is a direct consequence of the following statements. They can all be considerably generalized, but the current statements suffice for our purposes.

Proposition 2.2. *Let $\Omega \subset \mathbb{R}^n$ be a region which is topologically a closed n-ball B^n with a piecewise smooth boundary $\partial\Omega$ which is topologically an $n - 1$ sphere S^{n-1}. For every continuous nowhere vanishing vector field $F : \partial\Omega \to R^n - \{0\}$ there is a well-defined degree $\deg(F) \in \mathbb{Z}$ with the following properties.*

1. *The degree is constant in every continuous 1 parameter family F_s of non-vanishing vector fields i.e. for every continuous map*[1]

$$\hat{F} : \partial\Omega \times [0,1] \to \mathbb{R}^n - \{0\},$$

   where $F_s = \hat{F}|_{\partial\Omega \times \{s\}}$ and $F_0 = F$, the degree $\deg(F_s) = \deg(F)$ for all $0 \le s \le 1$.

2. *Suppose that $\tilde{F} : \Omega \to \mathbb{R}^n - 0$ is a continuous vector field which is continuously differentiable and transverse on the interior Ω° extending F, i.e. $\tilde{F}|_{\partial\Omega} = F$, the extension $\tilde{F}$ vanishes in isolated points $z_1, \ldots, z_m$ and its Jacobian matrix $D\tilde{F} : \Omega \to \mathbb{R}^{n \times n}$ is invertible at the zeroes z_i, then*

$$\deg(F) = \sum_i \operatorname{sign}(\det(D\tilde{F}(z_i))).$$

Note that a transverse smooth extension $\tilde{F}$ as in 2.2.2 always exists. These two statements allow us to count the number of equilibria. We use the notation of the beginning of section 2.4.2. For a proof of proposition 2.2, we refer to Appendix A.

We can *define* the number of equilibria counted with multiplicity as

$$\deg(F|_{S^2(V_0)})$$

for a large enough velocity V_0. See the discussion below assumption 2.1 for the meaning of large enough in the physical model. By proposition 2.2.2 we see that the degree has an interpretation as a number equilibria counted with multiplicity if the force vector field on the space of velocities is transverse, but we can always perturb F by an arbitrary small perturbation to get a transverse extension $\tilde{F}$. We also see that in the transverse case it is independent of V_0, as long as changing V_0 does not introduce new zeroes. We can always assume that the zeros of the transverse perturbation $\tilde{F}$ are all in a small neighborhood of the zeros of F to see that this is true in general.

We can compute the degree of $F|_{S^2(V_0)}$ using assumption 2.1 by deforming F to a vector field of which it is easier to compute the degree. We write v instead of $\vec{v}$. Let $F^{op} : v \to -1v$ be the force vector field which is always directed opposite to the velocity with a unit of proportionality that is 1 in suitable units. It is obviously nonzero on $S^2(V_0)$. Now define a one-parameter family $\hat{F} : S^2(V_0) \times [0,1] \to \mathbb{R}^3 - 0$ deforming F into F^{op} by

$$\hat{F}(v, s) = (1 - s)F(v) + sF^{op}(v) \tag{20}$$

It is obviously continuous and well defined as a family of vector fields. The reason it is non-vanishing on $S^2(V_0)$ is that for all $v \in S^2(V_0)$

$$v \cdot F_s = (1 - s)v \cdot F(v) + sv \cdot F^{op}(v) = (1 - s)v \cdot F(v) - sv \cdot v < 0 \quad \forall s \in [0,1]$$

We conclude that $\deg(F|_{S^2(V_0)}) = \deg(F^{op}|_{S^2(V_0)})$ and we only have to compute the latter. We can apply 2.2.2 to $F^{op}|_{S^2(V_0)}$ which is obviously already defined as a transverse vector field over the entire ball. Since we work in dimension 3

$$\deg(F^{op}|_{S^2(V_0)}) = \operatorname{sign}(\det(-1)) = \operatorname{sign}((-1)^3) = -1.$$

---

[1] Topologists call such a map a homotopy between F_0 and F_1

Actually this is cheating a bit, because to prove formula 2.2.2 we will to have to compute the degree of a linear vector field directly. In any case we conclude

Proposition 2.3. *Under the assumption 2.1 on the force vector field F, there are -1 equilibria counted with multiplicity on the ball $B^3(V_0)$ i.e.*

$$\deg(F|_{S^2(V_0)}) = -1.$$

3   Numerical analysis

3.1   Numerical Bifurcation Analysis of the Thruster Model

The scaling symmetry with respect to τ of the Thruster model means that the exact value of τ is not relevant. In addition, this is a toy model and so we somewhat randomly picked and fixed $\tau = 1000$.

All numerical computations in this section have been done with the continuation and bifurcation software AUTO [5]. We refer to the extensive manual for details. Here we only used the capabilities to solve algebraic equations with eigenvalue computation and detection of Hopf bifurcations, and to continue the branches of periodic solutions that emerge at such bifurcations. Fixing τ and the ship parameters from the 'Hamburg test case', the only parameter left in the Thruster model is the angle α, which is thus the primary bifurcation parameter in these computations.

Briefly, the idea of continuation is to numerically implement the implicit function theorem: given an equilibrium, parameter changes typically move the equilibrium along a smooth curve. In Section 3.3 we discuss a naive implementation of this idea with MATLAB. However, this naive approach fails at certain bifurcations and cannot resolve the bifurcating solutions, which is possible with AUTO. In particular, AUTO automatically computes the eigenvalues of the linearisation in the equilibria, which decide upon stability of the equilibrium. Hence, eigenvalue plots as given in Section 3.3 can also be made with AUTO, but we omit this here. In all plots of this section, solid lines correspond to stable solutions, dashed to unstable ones.

Notably, these steady state computations do not require to numerically solve the differential equation: we do not compute trajectories. The periodic solutions are computed automatically by the software. Therefore, these computations are extremely fast. For the simple three-dimensional ordinary differential equation used here the speed-up is modest, but it is dramatic for larger systems or partial differential equations. Moreover, this approach allows to detect unstable solutions, which is not possible by simulation. Knowing the location of unstable equilibria can be relevant, for instance, in order to find further stable equilibria or to apply a stabilizing control.

3.1.1   Stationary states by continuation from straight motion

In this section we present the result of continuation from the trivial straight motion equilibrium which was discussed in section 2.2.2. Recall symmetry (18) of (11), which will be inherited by the equilibrium branches – with branch we mean a curve of equilibria (or other types of solutions) and associated parameter values in the product of phase space and parameter (usually only α).
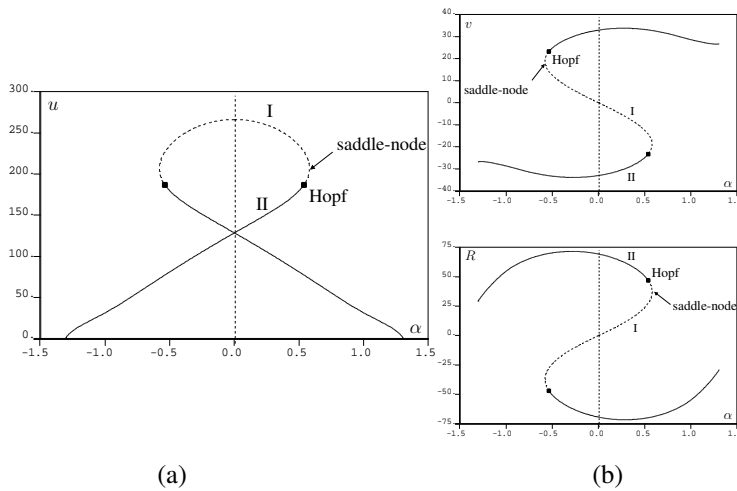
(a)   (b)

Figure 3: (a) The u-component of the branch of equilibrium solutions that connect to the straight motion. Dashed = unstable, solid = stable. Units of α are radians, units of u are m/s, but not meaningful for the random choice of $\tau = 1000$. (b) The other components of the equilibria shown in (a): upper panel v-components, lower panel R-components.

In Figure 3 we plot the numerical result from continuing the unstable straight motion equlibrium; this lies at the top of the dashed curve at $\alpha = 0$. In the following we describe the meaning of this figure and its interpretation for the ship motion, and refer to the labels I, II for the different sections along the branches in Figure 3(a).

Branch part I: Starting from the straight motion in either direction from $\alpha = 0$, the branch folds at $\alpha \approx \pm 0.58$, where saddle-node bifurcations take place and the equilibrium becomes unstable with respect to an additional real eigenvalues. The equilibrium is thus unstable in any (v, r)-direction. Further along the branch, these eigenvalues form a complex conjugate pair whose real parts cross zero at a Hopf-bifurcation.

Branch part II: Beyond the Hopf-bifurcation, the equilibria are stable and extend up to $\alpha \approx \pm 1.306$, which is about 75°. Notably, for each direction in α the branch crosses $\alpha = 0$ and thus there exist two stable equilibria at $\alpha = 0$, which do not have $v = r = 0$. Note that there are two stable and one unstable equilibria at $\alpha = 0$, which agrees with the predictions by degree theory 2.4.

At $u = 0$ the vector field is discontinuous, and it is therefore not surprising that the numerical continuation terminates at this value. Nevertheless, there exist other solution branches. See Section 3.1.3.

From Figure 3(b) we see that these equilibria have positive v- and negative r-components or vice versa. In particular, there are stable equilibria with positive thruster angle and rotation, which is at first counter-intuitive as the thrust points in the negative direction so that the sign should be opposite. Since the sideways velocity has this opposite sign, the hull motion is as expected, but the interaction of forces generates a rotation in the 'wrong' direction.

Thinking experimentally, this phenomenon occurs when first moving on an equilibrium circle with negative rudder angle and positive R on branch II, and then slowly increasing the rudder angle. The model predicts that even beyond straight rudder angle, the ship will still rotate in the direction it did before. However, when continuing this slow increase in α, at the Hopf-bifurcation the ship loses the ability to move in equilibrium and to rotate in the 'wrong' direction. In the next section we show that this is a subcritical bifurcation, which means that something 'dramatic' happens that the local bifurcation analysis cannot reveal. One possibility is that the motion settles to the other stable equilibrium with negative R and the overall dynamics follows a 'hysteresis' (see explanation below).

3.1.2   Periodic solutions emerging from primary Hopf bifurcation

In this subsection we discuss the branch of periodic solutions that bifurcates from the branch of steady states at the Hopf-bifurcation marked in Figure 3. See Figure 4. As mentioned, the bifurcation is subcritical, which means that the bifurcating periodic solutions are unstable so that the ship would not follow this trajectory by itself.

The branch of periodic solutions terminates at a homoclinic bifurcation, which means that the periodic profile 'collides' with an equilibrium: a homoclinic orbit is such that the trajectory converges in forward and backward time to the same equilibrium and makes an intermediate excursion. When approaching such a solution, the periodic orbits spend more and more time near equilibria which generates the characteristic profiles plotted in Figure 4(b). In the lower panel of this figure the gradients become large when the excursion from the equilibrium localises to a point because the period of all these plots is normalised to 1.

3.1.3   Other solution branches

The degree theory argument from Section 2.4 suggests that there exists at least one equilibrium for all angles α. Strictly speaking, this does not apply due to the discontinuity of the vector field at $u = 0$ and indeed, some new solutions are created when smoothing out the discontinuity as discussed at the end of this section. Nevertheless, the degree argument motivates to search for equilibria at angles $\alpha > 1.306$, which was the boundary from the previous section: $u = 0$ at $\alpha \approx 1.306$.

Using a root finder for larger values of α produces new solutions and thus the additional solution branches plotted in Figure 5. These are not connected to the branches already plotted in Figure 3 (due to the discontinuity at $u = 0$; see end of this section). Almost all of these solutions have negative u and may thus be less interesting for the application. One of the branches with positive u comes relatively close to the stable branch (marked by a circle) also in the r and v components, which suggests that the stable equilibria are somewhat more sensitive to perturbations for angles near $\alpha = 1.306$.

The rectangular region marked in Figure 5 contains several stable branches (with $u < 0$) and is enlarged in Figure 6(a). Notably, there co-exist two stable equilibria for all α between the vertical dotted lines, and these are connected by a branch of unstable equilibria. Such a configuration with two competing stable states is a signature of nonlinear systems, and also suggest vicinity of 'cusp' bifurcation. In practice this

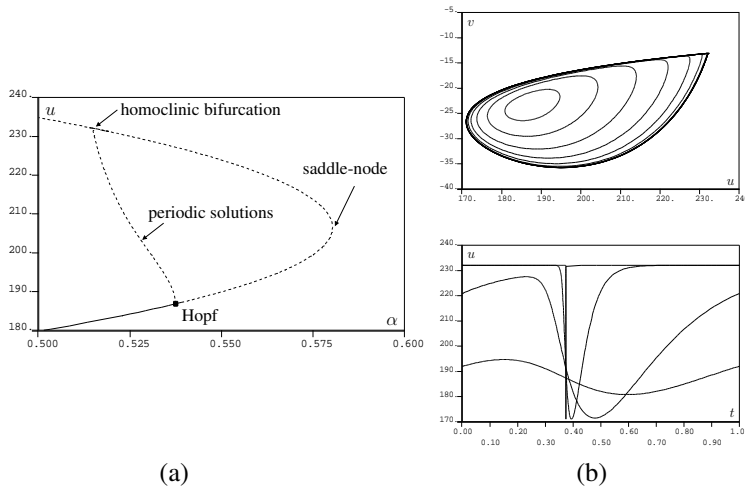|	
(a)	(b)

Figure 4: (a) Branch of periodic solutions that bifurcates from the steady state at the Hopf bifurcation, and terminates in a homoclinic bifurcation with background state at the upper end of the branch. (b) Plots of some periodic solutions along the branch in (a): upper panel (u, v)-space, lower panel (x, u)-space with period normalised to 1.

suggests that when starting with a ship making a stable circular motion from the upper branch and slowly increasing the thruster angle, the ship would suddenly jump (at the right dotted line) to another circular motion on the lower branch and the previous circular motion cannot be recovered by small modifications of the thruster angle. In order to jump back to the upper branch, the thruster angle would have to be moved back beyond the left dotted line. This phenomenon is called 'hysteresis'.

The rectangular region marked in Figure 6(a) is enlarged in Figure 6(b). It shows a supercritical Hopf bifurcation, where a branch of stable periodic orbits bifurcates. This branch terminates in a homoclinic bifurcation analogous to the case discussed in Section 3.1.2. (The plot is discontinuous because it shows the maximum u-value of the periodic solutions, while the equilibrium of the homoclinic bifurcation lies at the minimum.)

The role of the discontinuity of the hull force can be illustrated by replacing $\text{sign}(u)$ with, e.g., $2\arctan(u/\varepsilon)/\pi$ for small $\varepsilon > 0$. In Figure 7 we plot a comparison of this smoothing for $\varepsilon = 0.01$ with the discontinuous case. The branches in Figure 5 that are disconnected for the discontinuous case are connected for the smoothened case, and it seems that there are no further solutions. This would mean that in the discontinuous case there are intervals in α, e.g., $\alpha \sim 1.75$, for which there do not exist solutions. On the other hand, the fact that non-trivial solutions with $u = 0$ occur at all may be an artefact of the Thruster model. For the Rudder model, the forward thrust of the propeller should make this impossible, and indeed we do not find such solutions, as discussed in the next section.
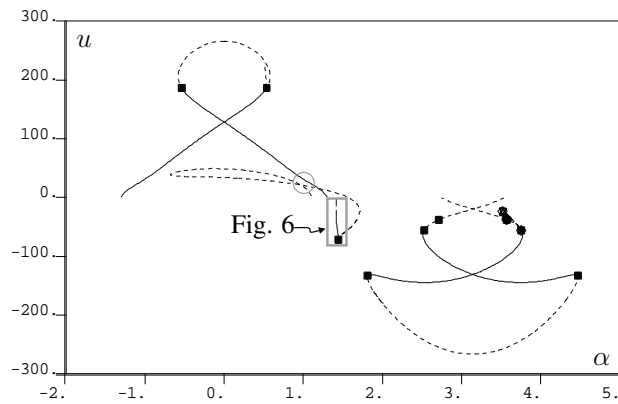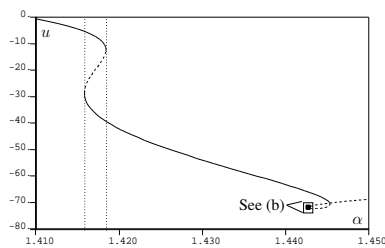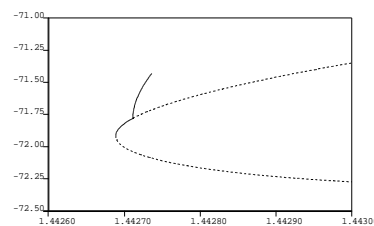
Figure 5: All the branches that have been found numerically. Additional branches arise from reflecting these about $\alpha = 0$.
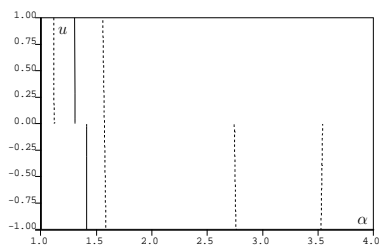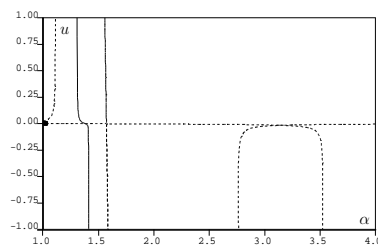

(a)

(b)

Figure 6: (a) Enlargement of the region marked in Figure 5. The S-shaped branch generates 'bistability': two different stable equilibria co-exist between the vertical dotted lines. (b) Enlargement of the region marked in (a). A branch of stable periodic orbits emerging in a Hopf bifurcation and terminating in a homoclinic bifurcation.

(a)

(b)

Figure 7: (a) Enlargement of a region near $u = 0$ of Figure 5. (b) The solutions for smoothened forces, replacing $\mathrm{sign}(u)$ by $2\arctan(100u)/\pi$.

3.2 Numerical Bifurcation Analysis of the Rudder Model

Analogous to the computations of the previous section, here we use AUTO to analyse numerically the non-dimensional 'Rudder model'. Note that in Section 3.3 below we present analogous, albeit less complete, results using a naive implementation of the continuation approach in MATLAB. The added value of the MATLAB routines is that these can automatically find equilibrium solutions (without a given good guess for one).

Similar to the scaling symmetry in τ of the Thruster model (11), here we have a scaling symmetry in the rate of rotation n of the propeller. Specifically, let $T_p(u; n)$ be the propeller force term T_p with explicit n-dependence. Then

$$T_p(\lambda u; \lambda n) = \lambda^2 T_p(u; n).$$

As mentioned for the Thruster model, the hull forces are homogenous of degree two, thus having the same scaling law as T_p. It is straightforward that also the rudder forces possess this homogeneity and therefore the entire right hand side does. Hence, it suffices to know solutions for one value of n, as the result for any other value follows from the above rescaling, as long as $n \neq 0$. For the numerical calculations we therefore fix $n = 2$.

In contrast to the Thruster model, this model has the two reflection symmetries

$$\begin{aligned}
(\delta, u, v, R) &\rightarrow (-\delta, u, -v, -R), \\
(90° + \delta, u, v, R) &\rightarrow (90° - \delta, u, -v, -R).
\end{aligned} \tag{21}$$

In particular, the model does not distinguish between the orientations of the rudder for a given angle. Due to the symmetries (21), the bifurcation diagrams are reflection symmetric about both $\delta = 0$ and $\delta = 90°$ (and thus also about $180°$). Another effect of neglecting the rudder orientation is that the branches of equilibria encountered here do not (need to) cross $u = 0$ so that these stay within the range of validity of the model. Recall N'_H is discontinuous at $u = 0$, and the branches in Figure 5 include $u = 0$. Indeed, the Thruster model (11) accounts for the direction of the rudder/thruster, and the branches in Figure 5 very roughly have the symmetry $(\alpha, u, r, v) \rightarrow (\pi + \alpha, -u, -r, -v)$.

3.2.1 Continuation from straight motion, and radii of rotation

In this section we use the parameter values of the Hamburg test case.

As for the Thruster model, a natural starting point for investigating equilibria is the straight motion where $\delta = v = r = 0$. In Figure 8 we plot the resulting branch of equilibria when varying δ. For small δ the result is qualitatively the same as for the Thruster model: straight motion is unstable and beyond folds (alias saddle-node bifurcations) around $\delta \approx \pm 1.5°$ there coexists a symmetric pair of stable branches 'bistability'. However, this range of angles is much smaller than in the Thruster model and there is no Hopf-bifurcation.

Branch part I: Beyond the folds, the branch is stable and has monotonically decreasing u-value until $\delta \approx \pm 75°$, while r and v behave non-monotonically both having a single extremum at $\delta \approx 28.5°$ (minimum for v, maximum for r). In contrast to the Thruster model there is no Hopf bifurcation in this range.
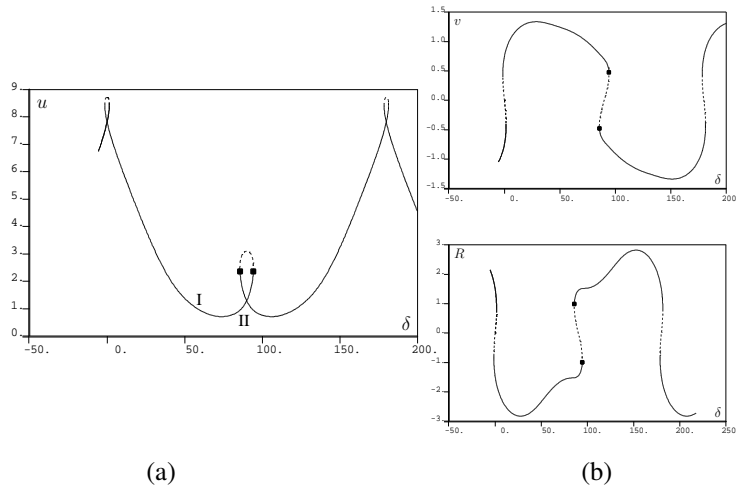
(a)   (b)

Figure 8: Branch of equilibria connected to the straight motion. (a) The u-component, (b) the v-component (upper panel) and R-component (lower panel). Recall that the components have units of m/s. The full branch consists of this part and the reflection about $\delta = 0$. The branch also has a reflection symmetry about $\delta = 90°$. Solid lines denote stable equilibria, dashed unstable ones. Squares denote Hopf bifurcations.
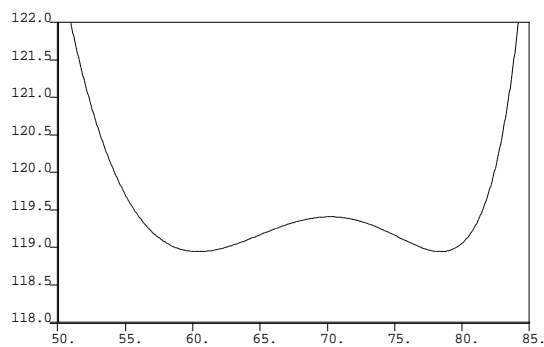

Figure 9: Radii, in m, of circle motion corresponding to part of the equilibrium branch in Figure 8. The remaining radii are monotone in δ: decreasing for small $\delta > 0°$ (from infinity at straight motion) and increasing for $85° < \delta < 90°$.

(a)   (b)
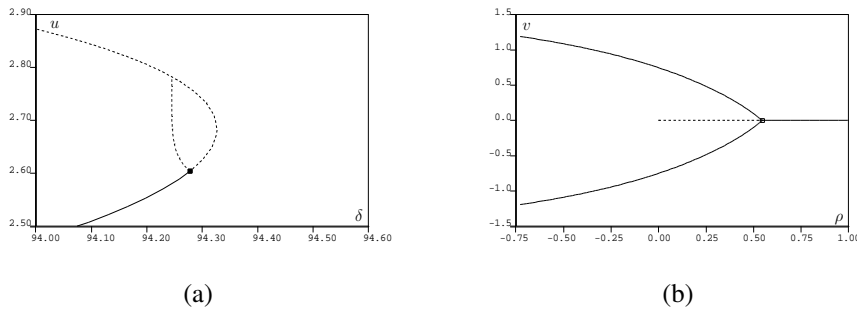
Figure 10: (a) Branch of periodic solutions emerging from a Hopf bifurcation. See Figure 8. It terminates in a homoclinic bifurcation. All periodic solutions are unstable. (b) Bifurcation diagram for changing rudder area $A_R^* = (1 + \rho)A_R$ with A_R from the Hamburg test case; note that $\delta = 0$ is fixed. The two stable branches emerging from the (degenerate) pitchfork bifurcation intersect $\rho = 0$ at the equilibria from the branch in Figure 8 at $\delta = 0$.

Part of the radii of the corresponding circular ship motion, given by $\sqrt{u^2 + v^2}/R$, are plotted in Figure 9. For smaller value of $\delta > 0$ the radii are monotone. Notably, this graph has two minima with essentially the same radii of ≈ 119m at quite different rudder angles δ. Hence, the smallest radius the ship of length 153m can make at equilibrium is roughly 75% its length. Note that the computations in Section 3.3 give the same results. See Figure 13.

Branch part II: Continuing further along the branch plotted in Figure 8, the u-components increase, and the equilibria undergo a Hopf bifurcation at $\delta \approx 94.28°$, as well as another fold at $\delta \approx 94.32°$. The branch of periodic solutions emerging at the Hopf bifurcation is plotted in Figure 10(a). It consists of unstable periodic solutions and the branch terminates in a homoclinic bifurcation, analogous to the cases discussed for the Thruster model.

3.2.2   Stability change of straight motion

Analogous to Section 2.2.3, where a mass parameter was changed in the Thruster model, here we change a parameter of the Hamburg test case set to stabilize straight motion in the rudder model. In this case we choose the rudder area A_R. As plotted in Figure 10(b), at roughly 1.5 times this rudder area, the straight motion becomes stable through a (degenerate) supercritical pitchfork bifurcation, much like in the Thruster model for the ship mass. A possible interpretation is that the intrinsic instability of the hull for straight motion can only be compensated by a sufficiently large rudder.

3.2.3   Other branches of equilibria: Sensitivity of stable motion

The numerical analysis with MATLAB presented in Section 3.3 shows existence of other equilibria than those connected to straight motion. Indeed, we can use AUTO to continue from these solution to reveal the entire branches, which are plotted in Figure 11. These branches form a symmetric pair of loops and all solutions on these
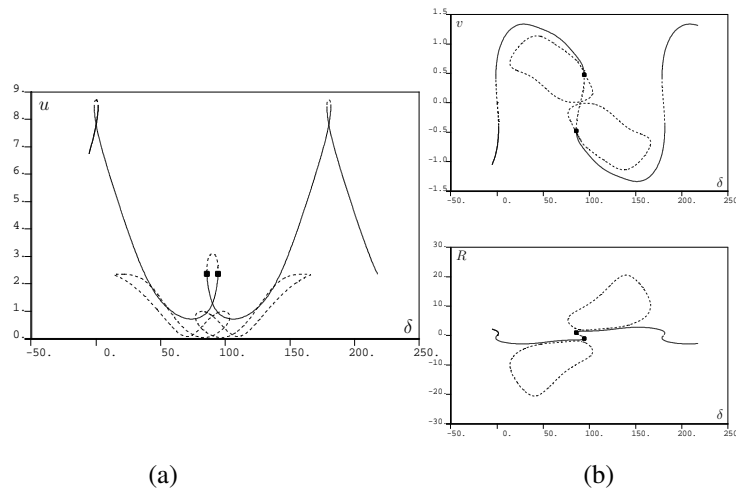
(a)   (b)

Figure 11: Bifurcation diagram of all known branches of equilibrium solutions. (a) The u-component, (b) the v-component (upper panel) and R-component (lower panel). In addition to Figure 8 here are two loops of unstable equilibria, symmetric about $\delta = 90°$. These loops have symmetric counterparts by reflection about $\delta = 0$ that are not shown.

symmetric branches are unstable.

A potential relevance of these solutions is their proximity to the stable branches for δ between $60°$ and $140°$. This suggests that the basin of attraction of the stable solutions becomes smaller for larger angles, that is, the stable motion is increasingly sensitive to perturbations. However, the basin of attraction, in particular for smaller δ, may be constrained by other nonlinear solutions that our analysis does not reveal.

3.3   Numerical Analysis of the Rudder Model using MATLAB

The results of Section 3.2 were computed using the program AUTO, which starts with one equilibrium solution of the equations of motion and from it computes a whole branch of solutions. We found the starting equilibrium solution for Figures 8–9 and 11 using MATLAB. In this section we describe in detail how the MATLAB program works. The MATLAB program not only finds equilibrium solutions to provide to AUTO, but also reproduces parts (but not all) of the bifurcation diagrams given in Section 3.2 and, like AUTO, determines whether or not the solutions are stable. We see a good agreement between the results of the two programs. In this section we present several eigenvalue figures. Note that AUTO also computes the eigenvalues, but we just do not show them in Section 3.2.

Model.   Recall that the (dimensional) equations of motion of the ship (1) have the form

$$\mathbf{M\dot{u}} = \mathbf{f(u; p)}, \tag{22}$$

where $\mathbf{u}$ is a vector of velocities and $\mathbf{M}$ is a matrix of mass and added mass coefficients:

$$\mathbf{u} = \begin{bmatrix} u(t) \\ v(t) \\ r(t) \end{bmatrix}, \quad \mathbf{M} = \begin{bmatrix} m + m_{uu} & 0 & 0 \\ 0 & m + m_{vv} & m_{vr} \\ 0 & m_{rv} & I_z + m_{rr} \end{bmatrix}. \tag{23}$$

The vector-valued function $\mathbf{f}$ is the nonlinear function of $\mathbf{u}$ defined by the right-hand side of equation (1) and it represents the resultant force on the ship:

$$\mathbf{f}(\mathbf{u}; \mathbf{p}) = \begin{bmatrix} mrv + X_G \\ -mru + Y_G \\ N_G \end{bmatrix}. \tag{24}$$

Note that $\mathbf{f}$ depends on the vector of control and design parameters $\mathbf{p}$. The control parameters are the rate of rotation of the propeller n and the rudder angle δ, and the design parameters, which are many, include the area, aspect ratio and position of the rudder, the diameter of the propeller, and the length and mass of the ship.

Stability theory. Suppose that the constant vector $\mathbf{u}_e = (u_e, v_e, r_e)^{\mathrm{T}}$ is an equilibrium solution of (22) for parameter vector $\mathbf{p}$, i.e., $\mathbf{f}(\mathbf{u}_e; \mathbf{p}) = 0$. Recall that equilibrium solutions of (22) correspond to straight motions of the ship if the rudder angle $\delta = 0$ and $v = r = 0$, or to turning circles otherwise. Standard results in the theory of ordinary differential equations (see, e.g., [10, Chapter 3] or [11, Chapter 9]) state that the stability of the equilibrium solution $\mathbf{u}_e$ is determined by the eigenvalues λ of the (generalised) eigenvalue problem

$$\mathbf{Df}(\mathbf{u}_e; \mathbf{p})\,\mathbf{v} = \lambda\,\mathbf{Mv}, \tag{25}$$

where $\mathbf{Df}(\mathbf{u}_e; \mathbf{p})$ is the Jacobian matrix of $\mathbf{f}$ evaluated at $(\mathbf{u}_e; \mathbf{p})$. It has components $[\mathbf{Df}]_{ij} = \partial f_i / \partial u_j$. The vector $\mathbf{v}$ is an eigenvector. (The eigenvalue problem (25) can be derived by linearising (22) about the equilibrium solution $\mathbf{u}_e$ and then seeking solutions with exponential time dependence $e^{\lambda t}$.) Recall that if all the eigenvalues λ of (25) have negative real part, then $\mathbf{u}_e$ is asymptotically stable. If at least one of the eigenvalues has positive real part (and the other eigenvalues have nonzero real part), then $\mathbf{u}_e$ is unstable.

Algorithm. We compute equilibrium solutions $\mathbf{u}_e$ and the corresponding eigenvalues λ in MATLAB in the following way: Fix the parameter vector $\mathbf{p}$. Starting from an initial guess $\mathbf{u}_0$, we solve the nonlinear algebraic equation $\mathbf{f}(\mathbf{u}_e; \mathbf{p}) = 0$ using the MATLAB function *fsolve*. The Jacobian matrix $\mathbf{Df}(\mathbf{u}_e; \mathbf{p})$ is then approximated using the centered difference formula. Finally, the eigenvalue problem (25) is solved using the MATLAB function *eig*. This computation takes a fraction of a second.

Parameter values. For our computations we took the design parameters of the ship to be fixed and equal to the values given in [7] for the Hamburg Test Case. For the wake fraction w and thrust deduction factor t, whose values are not given in [7], we took $w = 0.38$ and $t = 0.22$. For the control parameters, we took the rate of rotation of the propeller $n = 2$ Hz (number of rotations per second). We took the rudder angle δ to be the variable parameter and studied how the stability of equilibrium solutions depends on it.
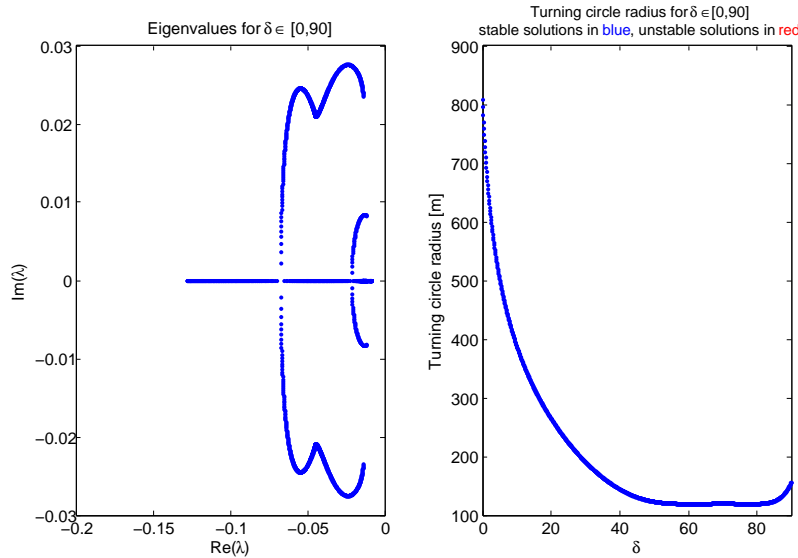
Figure 12: Results of Simulation 1. The graph on the left shows the eigenvalues corresponding to the equilibrium solutions for $\delta \in [0, 90]$ degrees (sampled every 0.1 degree). There are three eigenvalues per solution. Since all the eigenvalues lie in the left half-plane, all the equilibrium solutions are stable. The graph on the right shows the radius of the turning circle for each value of the rudder angle δ.

Results: Simulation 1, stable turning circles. Figures 12 and 13 show the results of the computation starting from initial guess $\mathbf{u}_0 \equiv (u_0, v_0, r_0) = (6\text{ ms}^{-1}, 1\text{ ms}^{-1}, 0$ radians·s$^{-1})$ for $\delta = 0$. We incremented δ in steps of 0.1 degrees from 0 to 90 degrees and every time we incremented δ we updated the initial guess $\mathbf{u}_0$, taking it to be the value of the equilibrium solution computed for the previous value of δ, i.e., $\mathbf{u}_0(\delta_{i+1}) = \mathbf{u}_e(\delta_i)$. To compute equilibrium solutions $\mathbf{u}_e$ and eigenvalues λ for the entire range of δ took around only 15 seconds. As seen from Figure 12, the program computes a family of *stable* turning circles (since all the eigenvalues lie in the left half-plane). The smallest turning circle has radius 118.94 m and is obtained at rudder angles $\delta = 60.4$ and $\delta = 78.4$ degrees. See Figure 13. Figure 13 agrees with the stable branch of the bifurcation diagram produced in AUTO (compare Figure 13 with Figures 8–9).

Results: Simulation 2, branch jumping. In this simulation we show the importance of the initial guess $\mathbf{u}_0$ in determining which branches of solutions the MATLAB program finds. This time we keep the initial guess fixed at $\mathbf{u}_0 \equiv (u_0, v_0, r_0) = (6$ ms$^{-1}, 1$ ms$^{-1}, 0$ radians·s$^{-1})$, the same initial guess that was used in Simulation 1 for $\delta = 0$, for all values of $\delta \in [0, 40]$ degrees; we do not update the initial guess when we update δ. The results are shown in Figures 14 and 15. Observe that for δ between 30 and 40 degrees, the program jumps between a stable and a nearby unstable branch of turning circle solutions. The stable branch is the same one that was produced in Simulation 1. We use a point on the unstable branch as the starting point
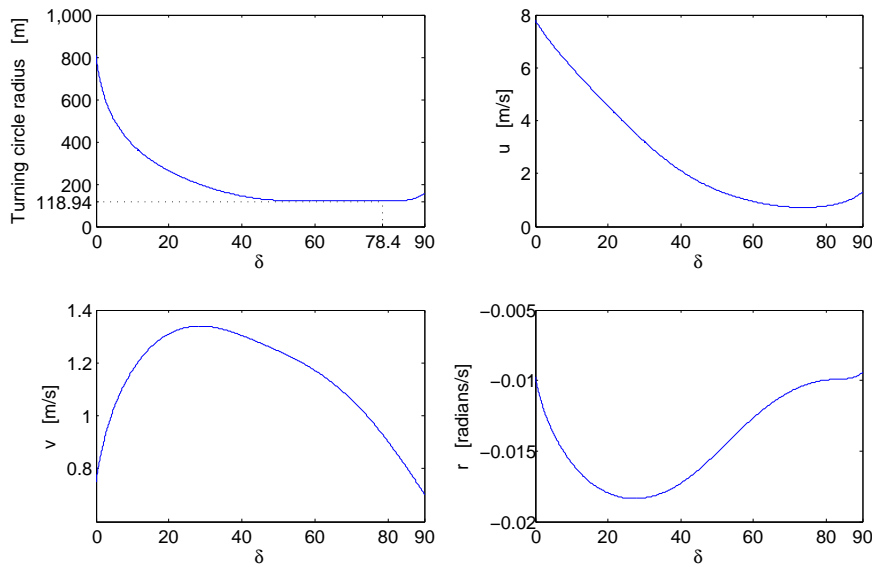
Figure 13: Results of Simulation 1. The turning circle radius and velocity components of the ship for rudder angles $\delta \in [0, 90]$.
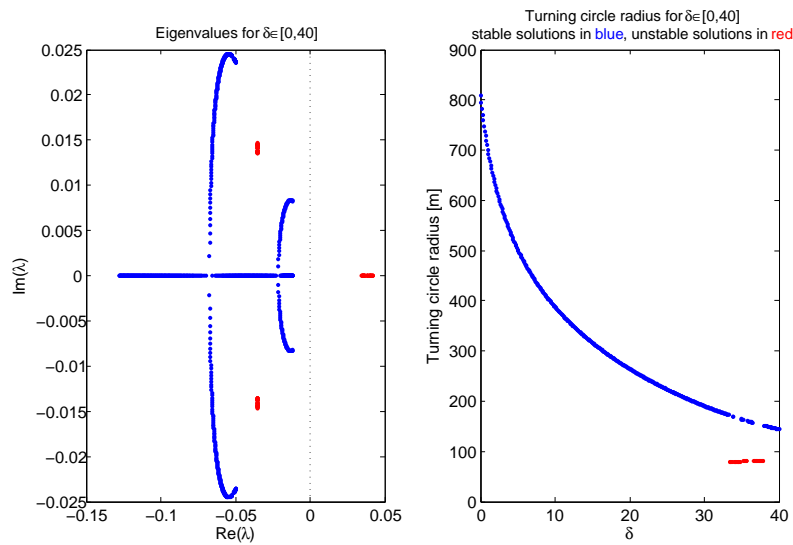

Figure 14: Results of Simulation 2. The graph on the left shows the eigenvalues corresponding to the equilibrium solutions for $\delta \in [0, 40]$ degrees. The nonlinear solver jumps between a stable and an unstable branch of solutions. The eigenvalues of stable solutions are blue and those of unstable solutions are red. The graph on the right shows the radius of the turning circle for each value of the rudder angle δ.
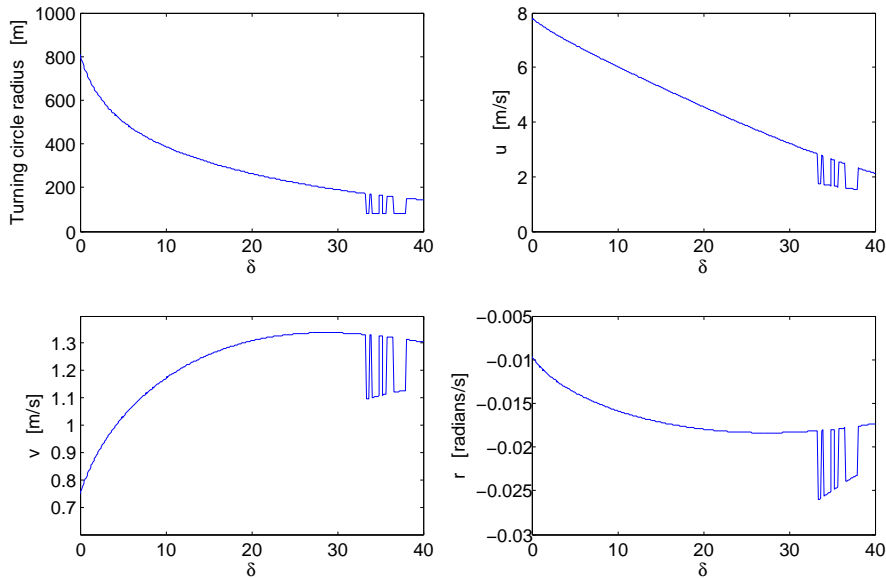
Figure 15: Results of Simulation 2. The discontinuities in the graphs are due to the nonlinear solver jumping between stable and unstable solution branches.

for Simulation 3.

Results: Simulation 3, unstable turning circles. In this simulation we produce an unstable branch of turning circle solutions for $\delta \in [37, 90]$ degrees. For $\delta = 37$ degrees, we take the initial guess $\mathbf{u}_0$ to be the solution computed in Simulation 2 for $\delta = 37$. We then update this initial guess every time that δ is incremented, as in Simulation 1. The results are shown in Figures 16 and 17. In this case we see that every equilibrium solution computed is an unstable turning circle. The smallest turning circle has radius 63.74 m, which is smaller than the smallest turning circle computed in Simulation 1. Since the solution here is unstable, however, it would be impossible for the ship to perform the smaller turning circle. The complete unstable branch, of which Figure 17 forms a part, was computed in AUTO. Compare Figure 17 to Figure 11.

Summary and Remarks. Our MATLAB program is a fast way of computing equilibrium solutions of the equations of motion, determining their stability, and finding the smallest possible turning circle that a ship can perform. This algorithm is far quicker than time-integrating the equations of motion. In the simulations above we chose to fix the design parameters of the ship and the propeller speed, and to vary the rudder angle. The program, however, allows any of the parameters to be varied. For example, the user could study the effect of varying the rudder area on the turning circle manoeuver.
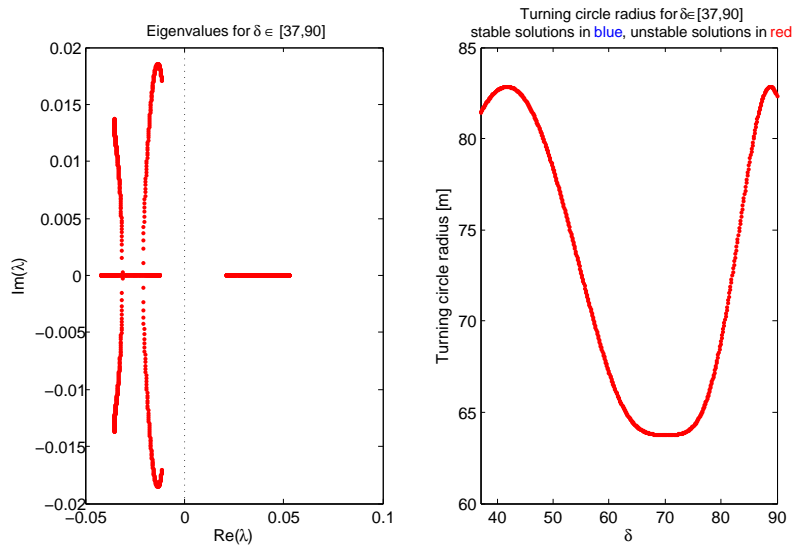
Figure 16: Results of Simulation 3. The graph on the left shows the eigenvalues corresponding to the equilibrium solutions for $\delta \in [37, 90]$ degrees. Every solution has one eigenvalue in the right half-plane and so all the solutions are unstable. The graph on the right shows the radius of the turning circle for each value of the rudder angle δ.
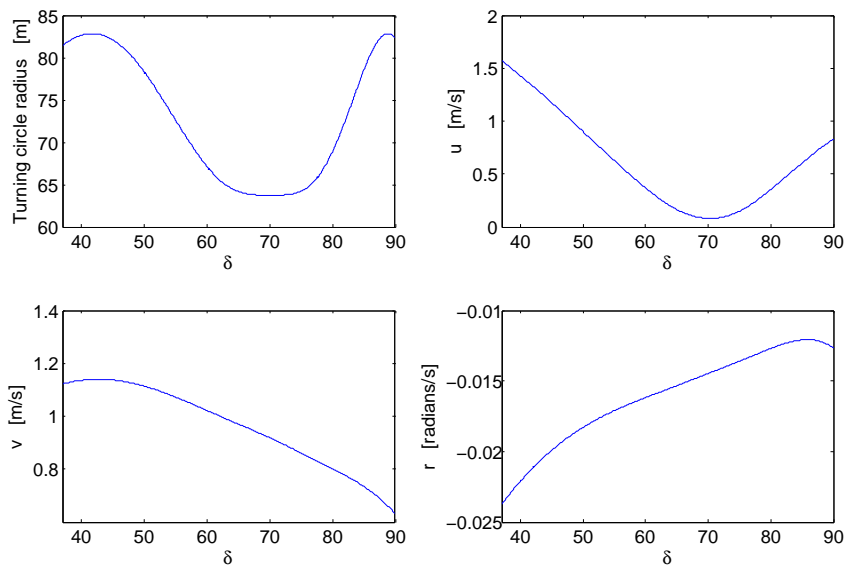

Figure 17: Results of Simulation 3. The turning circle radius and velocity components of the ship for rudder angles $\delta \in [37, 90]$. All these solutions are unstable.

4 Discussion & Outlook

We have numerically and theoretically analyzed the 'Rudder model' for ship manoeuvering provided by MARIN, and introduced a simplified 'Thruster model' that roughly combines rudder and propeller. We have shown that steady states in the model correspond to circular motion of the ship and computed the corresponding radii. We have non-dimensionalized the models and thereby remove a number of parameters, so that, due to a scaling symmetry, only the rudder (or thruster) angle remain as a free parameter.

Using 'degree theory', we have shown that a slight modification of the models possesses at least one steady state for each angle, and we have found certain constraints on the possible steady state configurations regarding stability.

We have shown that straight motion is unstable for the Hamburg test case and have used numerical continuation and bifurcation software to compute a number of curves of states together with their stability, and the corresponding radii of the ship motion. In particular, for the Rudder model straight forward motion can be stabilized by increasing the rudder size parameter, and the smallest possible radius is ~ 119 m. For the Thruster model we show that this also works when decreasing the ship weight parameter.

These analyses have illustrated methods and tools from nonlinear dynamical systems theory that can be used to analyse a model without simulation. Compared with simulations, the numerical bifurcation analysis is much less time consuming. We have implemented the model in MATLAB and provide a simplistic continuation method. The advanced continuation and numerical bifurcation analysis has been done with an implementation of the model in the software AUTO.

In conclusion, it is indeed possible to analyse the manoeuvring behavior of a ship, both in a qualitative sense and in a quantitative sense, based on the mathematical model alone, without the need for explicit solutions from by time integration methods.

As an outlook, we remark that it is possible to automatize much of the numerical computation in order to make these techniques available to non-experts. This could lead to a more generic design tool which allows the formal definition of the manoeuvring equations, the specification of the coefficients and the definition of the design input and output parameters (e.g. turning circle diameter vs rudder angle).

It is also possible to devise and analyse control techniques that stabilize a desired course of the ship. On the other hand, the analysis in this report does not cover the modified rudder forces for other courses than straight ahead.

A   Appendix: The topological degree

In this appendix, we will give some more information on the topological degree and we will explain and prove Proposition 2.2.

To define the degree of 2.2 there are various possibilities. The best way is to use homology and cohomology theory. Unfortunately this requires (even) more machinery than we want to use here. Instead we use the *homotopy groups* which are comparatively easy to define and easy to compute for the case we need it, even though they are subtle and difficult to compute in general. We also use *differential forms*, which are very concrete objects whose calculus is a generalization of classical vector calculus but *much* easier to compute with, both for people and computers. The material in this section is standard but the presentation of 2.2.2 is a rehash of folklore and simplifications of more general constructions. A quick introduction to differential forms is in [3], [9] and in the nice little book [2]. Their relation to topology is in the equally nice [1], and to numerical mathematics (aka discrete exterior calculus) in [4] . More topology can be found in [8] and [6].

The n-th homotopy group $\pi_n(X)$ of a space X, is the set of *equivalence classes* of continuous maps $\sigma : S^n \to X$ of the n-sphere to X.[2] Two maps $\sigma_1, \sigma_2 : S^n \to X$ are *equivalent* if one can be deformed in the other with a 1 parameter family σ_s, a so called homotopy. The idea is that once everything that can be deformed by continuous deformations is equivalent, what is left is something discrete and (more) computable. Two maps σ_1 and σ_2 can be juxtaposed (in dimension 1 this is running one path after the other), and this defines a composition map on $\pi_n(X)$. The neutral element is the map that sends a sphere to a point in X and the inverse of the composition is given by precomposing with reflection in a plane (or equivalently, any orthogonal map with determinant -1; in dimension 1, this corresponds to running a path backwards). The upshot is that $\pi_n(X)$ is a group for $n \geq 1$ and an Abelian group for $n \geq 2$. Moreover for every continuous map $f : X \to Y$ there is a map $f_* : \pi_n(X) \to \pi_n(X)$ by post-composition i.e. given a map $\sigma : S^n \to X$ defining an equivalence class $[\sigma] \in \pi_n(X)$ we define $f_*[\sigma] \in \pi_n(Y)$ as the equivalence class of $f \circ \sigma : S^n \to X \to Y$. One easily checks this is well defined. It is also easy to check that $(f \circ g)_* = f_* \circ g_*$ (functoriality), that f_* is a group homomorphism and that f_* only depends on the homotopy class of f. We find in particular that if $i : X \hookrightarrow Y$ is a subspace and there is a projection $p : Y \to X$ which is homotopic to the identity, then $i_* : \pi_n(X) \xleftarrow{\cong} \pi_n(Y)$ is an isomorphism. In particular we see that

$$i_* : \pi_n(S^m) \cong \pi_n(\mathbb{R}^m - \{0\}) \tag{26}$$

To actually compute the homotopy groups is not at all easy, in fact it is an active research area to compute and understand the higher homotopy groups of simple spaces like the n-sphere. However, the following is a very well-known and basic theorem of algebraic topology,

$$\pi_k(S^n) \cong 0 \text{ for } 1 \leq k < n \tag{27}$$
$$\cong \mathbb{Z} \text{ for } k = n \tag{28}$$

---

[2]This is a slight oversimplification, we have to map base-points to base-points, for example to define addition. Here we can ignore this

Note that the identity map gives a canonical generator for the group $\pi_n(S^n)$.

We can now define the degree of a continuous vector field $F : S^{n-1} \to \mathbb{R}^n - \{0\}$. The vector field defines a group homomorphism

$$F_* : \pi_{n-1}(S^{n-1}) \cong \mathbb{Z} \to \pi_{n-1}(\mathbb{R}^n - \{0\}) \cong \pi_{n-1}(S^{n-1}) = \mathbb{Z}.$$

Group homomorphism $\phi : \mathbb{Z} \to \mathbb{Z}$ are very concrete things because they are just multiplication by the integer $\deg(\phi) = \phi(1)$. For example

$$\phi(3) = \phi(1 + 1 + 1) = \phi(1) + \phi(1) + \phi(1) = 3\phi(1) = 3\deg(\phi).$$

We define

$$\deg(F) = \deg(F_*).$$

We now turn to the calculus of differential forms. An elementary differential form of dimension k on an open set $U \subset \mathbb{R}^n$ is a formal expression of the form

$$dx^{i_1} \wedge dx^{i_2} \wedge \cdots \wedge dx^{i_k}$$

a differential form ω is a sum of elementary differential forms with function coefficients i.e.

$$\omega = \sum_{i_1,\ldots,i_k} \omega_{i_1,\ldots,i_k}(x_1,\ldots,x_k)dx^{i_1} \wedge dx^{i_2} \wedge \cdots \wedge dx^{i_k}$$

In the following we will assume the function coefficients $\omega_{i_1,\ldots,i_k}(x_1,\ldots,x_k)$ to be smooth. The wedge product $\wedge$ in an elementary differential form is associative but it anti-commutes:

$$dx^i \wedge dx^j = -dx^j \wedge x^i.$$

We can thus assume that the indices are all different. If the set $\{i_i,\ldots i_k\} \neq \{j_1,\ldots j_k\}$, then $dx^{i_1} \wedge \cdots \wedge dx^{i_k}$ is independent of $dx^{j_1} \wedge \cdots \wedge dx^{j_k}$. The interpretation is that differential forms keep track of what flows through an infinitesimal surface or volume element in a certain direction (of which there can be many). For example the 2 form

$$j = j_{12}dx \wedge dy + j_{23}dy \wedge dz + j_{31}dz \wedge dx \tag{29}$$

has a natural physical interpretation as a current with e.g. $j_{23}dy \wedge dz$ the amount of mass (or charge or energy...) per unit time flowing through an infinitesimal part of the oriented y-z plane and it correspondingly has units of kg/sec (or Cb/sec, or J/sec ...) rather than kg/(sec m^2).

We can *pull back* a differentiable form with a smooth map $f : V \to U$, where $V \subset \mathbb{R}^m$ to get a new k form $f^*\omega$ on V. What this means is that if we write the map f in coordinates as

$$f(y_1,\ldots,y_m) = (x^1(y_1,\ldots,y_m),\ldots,x^n(y_1,\ldots y_k)$$

then we use linearization to expand $dx^i = \sum_j \frac{\partial x^i}{\partial y^j}dy^j$ and multiply everything out using the anti-commutativity of the wedge product. What we get is an expression which "simplifies" in a expression in determinants of minors of the Jacobian and elementary differential forms $dy^{j_1} \wedge \cdots dy^{j_k}$ with $j_1 < \cdots < j_k$. It is easy to see that

if $g : W \to V$ is another smooth map, then $(f \circ g)^* = g^* \circ f^*$(another instance of functoriality).

What makes this useful is that forms can be integrated over an oriented smoothly embedded k-simplex $\sigma : \Delta_k \to U$.

$$\int_\sigma \omega = \int_{\Delta_k} \sigma^* \omega = \int_{\Delta_k} \sum \omega_{i_1,\ldots,i_k} \det \left(\frac{\partial(x^{i_1}, \ldots, x^{i_k})}{\partial(t^1, \ldots t^k)} \right) dt^1 \wedge \cdots \wedge dt^k$$

where the last expression can be interpreted using normal Riemann or Lebesgue integration. The integral is independent of the curvilinear coordinates we use, because the forms keep track of all the necessary Jacobians, which is the point of introducing them. We can therefore extend the definition of integration of a k form over smoothly embedded oriented k dimensional compact sub-manifolds $\sigma : K \to U$, by triangulation.

The other thing to know about differential forms is Stokes's formula, a better behaved, and more user friendly generalization of the Gauss and Stokes formulas. Define the exterior derivative d as

$$d\omega = \sum_{j,i_1,\ldots i_k} \frac{\partial \omega_{i_1,\ldots i_k}}{\partial x^j} dx^j \wedge dx^{i_1} \wedge \cdots \wedge dx^{i_k}.$$

It commutes with pullback i.e. $d(f^*\omega) = f^* d\omega$. In particular, with the exterior derivative we can change curvilinear coordinates at will, unlike the classical divergence and curl which work different in rectangular and spherical coordinates. The exterior derivative therefore works fine on smooth manifolds. Now for a piecewise smooth k-dimensional manifold M with boundary ∂M we have

$$\int_{\partial M} \omega = \int_M d\omega \tag{30}$$

For example for the 2-form current j of (29), and $M \subset \mathbb{R}^3$, equation (30) boils down to

$$\int_{\partial M} j = \int_M (\partial_z j_{12} + \partial_x j_{23} + \partial_y j_{31}) \, dx \wedge dy \wedge dz$$

in which we recognize the classical Gauss formula.

It follows from Stokes formula that if $\sigma : S^{n-1} \to \mathbb{R}^n - \{0\}$ and $\sigma' : S^{n-1} \to \mathbb{R}^n - \{0\}$ are smoothly homotopic smooth maps and ω is a form on $\mathbb{R}^n - 0$ with $d\omega = 0$ (a so called closed form), then

$$\int_\sigma \omega = \int_{\sigma'} \omega$$

One can show that the homotopy classes of spheres $\pi_n(S^n)$ are represented by smooth maps and that for smooth maps, equivalence up to smooth homotopies is the same as equivalence up to continuous homotopies. Thus it makes sense to integrate over homotopy classes and it is then easy to see that $\int_{k[\sigma]} \omega = k \int_\sigma \omega$. This will allow us to compute degrees and prove the local to global degree formula 2.2.2[3]

---

[3]This construction is a version of the de Rham cohomology construction of the localised Euler class. See [1].

For notational simplicity we set $n = 3$. Choose a form ω written in spherical coordinates on $\mathbb{R}^3 - \{0\}$ as $\omega = f(\phi, \theta)d\phi \wedge d\theta$ such that

$$\int_{S^2} \omega = 1.$$

For example we could take $f(\phi, \theta) = -\sin(\theta)$, but we could also take f to be a bump function with support near $(\phi, \theta) = (0, \pi/2)$, and it is interesting to compare the interpretation of the results below. Clearly $d\omega = 0$ because there is no r-derivative and, say, the θ-derivative comes with a $d\theta$, but $d\theta \wedge d\theta = 0$. Now for a smooth vector field $F : S^2 \to \mathbb{R}^3 - \{0\}$, we have

$$\deg(F) = \deg(F) \int_{S^2 \subset \mathbb{R}^3 - \{0\}} \omega = \int_{F_*(S^2(V_0))} \omega = \int_{S^2(V_0)} F^*\omega$$

Suppose further that F is continuously differentiable and non-vanishing on $\Omega - Z_\epsilon$ where Z_ϵ is an ϵ neighborhood of the zeroes of X with smooth boundary and $\partial\Omega = S^2$.

$$\begin{aligned}
\deg(F) &= \int_{S^2} F^*\omega \\
&= \int_{\partial(\Omega - Z_\epsilon)} F^*\omega + \int_{\partial Z_\epsilon} F^*\omega \\
&= \int_{\Omega - Z_\epsilon} F^* \underbrace{d\omega}_{0} + \int_{\partial Z_\epsilon} F^*\omega \\
&= \int_{\partial Z_\epsilon} F^*\omega
\end{aligned}$$

Now finally assume that F is continuously differentiable on Ω and transversal with isolated zeros in $z_1, \ldots z_m$. Then ∂Z_ϵ is a union of small 2-spheres $S_1^2(\epsilon), \ldots S_m^2(\epsilon)$. If the 2-spheres $S_i^2(\epsilon)$ are chosen small enough, then on $S_i^2(\epsilon)$ $F(x) = L_i(x) + o(\epsilon)$ where $L_i(x) = (DF)_{z_i}(x - z_i)$ is the linearization of F around z_i. The Jacobian $(DF)_{z_i}$ is invertible (by definition of transversality), so by compactness of $S^2(\epsilon)$, $|L_i(x)| \geq c\epsilon$. Hence, the rest term can be estimated on $S^2(\epsilon)$ as $o(\epsilon) < 1/2|L_i(x)|$ for ϵ sufficiently small. We can therefore make a linear homotopy of the restriction $F|_{S_i^2(\epsilon)}$ to the linearization $L_i|_{S_i^2(\epsilon)}$ similar to (20). We conclude that

$$\begin{aligned}
\deg(F) &= \int_{\partial Z_\epsilon} F^*\omega \\
&= \sum_i \int_{S_i^2(\epsilon)} F^*\omega \\
&= \sum_i \int_{F_*(S_i^2(\epsilon))} \omega \\
&= \sum_i \int_{L_i*(S_i^2(\epsilon))} \omega
\end{aligned}$$

But the degree of a linear vector field $x \to Ax$ with A invertible, depends only on the sign of $\det(A)$ i.e. the connected component of $\mathrm{GL}(n, \mathbb{R})$ containing A. We finally conclude that

$$\deg(F) = \sum_i \mathrm{sign}(\det((DF)_{z_i})). \tag{31}$$

References

[1] R. Bott and L.W. Tu. *Differential forms in algebraic topology*. Springer, 1982.

[2] T. Bröcker and K. Jänich. *Introduction to differential topology*. Cambridge University Press, 1982.

[3] Y. Choquet-Bruhat, C. DeWitt-Morette, and M. Dillard-Bleick. *Analysis, manifolds, and physics*. North-Holland, 1982.

[4] M. Desbrun, A.N. Hirani, M. Leok, and J.E. Marsden. Discrete exterior calculus. *Arxiv preprint math/0508341*, 2005.

[5] E. Doedel, R.C. Paffenroth, A.R. Champneys, T.F. Fairgrieve, Y.A. Kuznetsov, B.E. Oldeman, B. Sandstede, and X. Wang. Auto2000: Continuation and bifurcation software for ordinary differential equations (with homcont). *Technical report, Concordia University*, 2002.

[6] A. Hatcher. *Algebraic topology*. Cambridge Univ Press, 2002.

[7] MARIN. *Studiegroep Wiskunde met de Industrie 2011. MARIN - Manoeuvring Behaviour of Ships. Report No.: SWI-MARIN*. January 2011.

[8] J.R. Munkres. *Elements of algebraic topology*. Westview Press, 1984.

[9] R. Sjamaar. Manifolds and Differential forms. *Lecture Notes, Cornell University*, 2001.

[10] C.J. van Duijn and M.J. de Neef. *Analyse van Differentiaalvergelijkingen*. VSSD, 2001.

[11] Boyce W.E. and DiPrima R.C. *Elementary Differential Equations*. Wiley, 8th edition, 2004.